Charge transfer hybrids of graphene oxide and the intrinsically microporous polymer PIM-1

Article (Accepted Version)

Charge Transfer Hybrids of Graphene Oxide and the Intrinsically Microporous Polymer PIM-1

Yuanyang Rong [1], Matthew J. Large *[1], Manoj Tripathi [1], Sean P. Ogilvie [1], Aline Amorim Graf [1], Boyang Mao [2], Jacob Tunesi [1], Jonathan P. Salvage [3], Alice A. K. King [1], Alessia Pasquasi [1], Marco Peccianti [1], Richard Malpass-Evans [4], Neil B. McKeown [4], Frank Marken [5] and Alan B. Dalton *[1]

[1] School of Physics and Astronomy, University of Sussex, Brighton, BN1 9RH, UK

[2] National Graphene Institute, University of Manchester, Booth Street East, Manchester M13 9PL, UK, University of Manchester

[3] School of Pharmacy and Biomolecular Science, University of Brighton, Brighton BN2 4GJ

[4] School of Chemistry, University of Edinburgh, West Mains Road, Edinburgh, EH9 3JJ, UK

[5] Department of Chemistry, University of Bath, Claverton Down, Bath, BA2 7AY, UK

Keywords: graphene oxide, microporous polymers, nanoparticles, charge transfer, catalysis

Abstract: Nanohybrid materials based on nanoparticles of the intrinsically microporous polymer PIM-1 and graphene oxide (GO) are prepared from aqueous dispersions with a re-precipitation method, resulting in the surface of the GO sheets being decorated with nanoparticles of PIM-1. The significant blueshift in fluorescence signals for the GO/PIM-1 nanohybrids indicates modification of the optoelectronic properties of the PIM-1 in the presence of the GO due to their strong interactions. The stiffening in the Raman G peak of GO (by nearly 6 cm^{-1}) further indicates p-doping of the GO in the presence of PIM. Kelvin probe force microscopy (KPFM) and electrochemical reduction measurements of the nanohybrids provide direct evidence for charge transfer between the PIM-1 nanoparticles and the GO nanosheets. These observations will be of importance for future applications of GO-PIM-1 nanohybrids as substrates and promoters in catalysis and sensing.

Introduction

Charge transfer processes on the nanoscale play a key role in a range of organic electronic devices such as solar cells[1], light emitting diodes[2] and field-effect transistors[3, 4]. The efficiency of charge transfer at the interfaces between the electron-donating and electron-accepting materials is critical to the performance of such devices. The effect of charge transfer is also observed in the fields of sensing and catalysis[5]. In particular, the charging effect between the individual component[5] and the substrates[6] could facilitate the formation of conductive phases thus further promoting the catalytic efficiency[7].

Polymers of intrinsic microporosity (PIMs) have emerged as a novel class of material in a range of applications including gas permeation[8-10], gas separation[8, 9] and hydrogen storage[8]. In particular, a polybenzodioxane polymer, PIM-1, the first synthesized soluble and processable PIM (see structure in Figure 1A), due to its conjugated nature, exhibits strong fluorescence and is solution processable allowing it to be cast as a transparent, yellow-tinted freestanding film. Recently, it has been suggested that PIM-1 possesses n-type semiconductor characteristics and efficient electron charge transport for low cost and flexible polymer light-emitting diodes (PLEDs)[11]. Moreover, PIM-1 exhibits molecularly rigid and constrained structures leading to microporosity, which make it a useful material for heterogeneous catalysis[12]. Introduction of other materials to form the hybrids seems to be a feasible route to further understand and improve the properties of PIM-1.

However, to the best of our knowledge, the nanoscale electronic properties and the associated optical signature of the PIM-1 nanohybrids have never been reported.

Graphene oxide (GO) is usually employed as a precursor for the large-scale production of graphene[13] because of two important characteristics, solution processability from aqueous colloidal dispersions and synthetic accessibility from inexpensive raw graphite. Recently, GO has been highlighted not only for its relevance to graphene production, but also for its own unique chemical structure and characteristics, which enable new applications in fields like catalysis, electronics, and optolelectronics[14]. One of the most interesting properties of GO related is its heterogeneous electronic structure, which results from the existence of both sp^2 and sp^3 hybridized carbon atoms[15] in an atomically thin 2D nanosheet. The presence of functional groups on the basal plane and at edges of GO allow interaction with a range of chemicals through either covalent or non-covalent bonds to produce nanohybrid materials with novel properties[16]. The charge-transfer phenomena between graphene and conjugated polymers has been extensively reported and the resulting nanohybrids exhibit enhanced conductivity and better efficiency, for example in photovoltaic devices[17–19]. However, the interesting properties of graphene oxide nanohybrids with polymer systems are only beginning to emerge. In previous work,[20] we employed the re-precipitation approach to prepare conjugated polymer/GO nanohybrids to facilitate the intimate contact between both materials. These nanohybrids were found to exhibit interesting charge transfer behavior. Hence, it is of great interest to apply this same approach to develop novel GO-functionalized or nanohybrid materials and to understand and tailor nanohybrid properties. Previous work on hybridization of graphene oxide and polymers of intrinsic microporosity has been sparse. Graphene oxide has been incorporated into PIM-1 membranes with enhanced gas transport and gas separation performance[21–22,] but the nanoscale interactions between these two materials have not previously been investigated. Here, a novel type of nanohybrid is studied based on these two interesting materials, graphene oxide and the fluorescent polymer of intrinsic microporosity (PIM-1) in order to reveal the inherent electronic properties.

In this paper, we demonstrate the presence of localised charge transfer effects based on extensive characterization of GO/PIM-1 nanohybrids (illustrated in Figure 1). The nanohybrid materials were fabricated in water dispersions with varying GO concentration. The structural morphology was characterized by scanning electron microscopy (SEM) and atomic force microscopy (AFM). UV-visible photoluminescence (both steady-state and time-resolved), and Raman spectroscopies were employed to understand the interaction and resultant optoelectronic properties. Electrochemical measurements were performed to characterize the ease of reduction of GO to graphene as a function of PIM-1 polymer content. It is illustrated that charge transfer in the nanohybrid materials is likely to cause tuning of some spectroscopic and surface properties for both GO and PIM-1. This opens up opportunities for further exploration in particular for microporous nanocomposites as substrates/promoters for catalysis and for sensing.

Experimental section

Chemical Reagents

Polymer PIM-1 was prepared following a literature recipe; the dibenzodioxane formation reaction was performed using the commercially available bis-catechol 5,5',6,6'-tetrahydroxy-3,3,3',3'-tetramethyl-1,1'-spirobisindane and 2,3,5,6-tetrafluroro-terephthalonitrile[9]. Graphene oxide in aqueous dispersion (25 mg/mL) was obtained from Graphenea (San Sebastián, Spain) (flake size ~10 um, monolayers, C/O ratio~2.1). Tetrahydrofuran, phosphoric acid (85%) and sodium hydroxide were purchased from Fisher Scientific and used without further purification. Solutions were prepared with deionized water of resistivity of 18.2 MΩ·cm freshly prepared using a Thermo Scientific Barnstead Smart2Pure purifier.

Synthesis of GO-PIM-1 nanohybrid materials in dispersion

PIM-1 nanoparticles and GO/PIM-1 nanohybrids were synthesised using the re-precipitation method. A volume of 1 mL PIM-1 in THF solution (1 mg/mL) was added into 20 mL GO water dispersion (GO weight, 0 mg, 0.5 mg, 1 mg, or 2 mg) drop-by-drop under vigorous stirring (6000 rpm for 10 mins) in a Silverson LM5-A high shear mixer. The GO/PIM weight ratios in the resulting nanohybrid dispersions in water were 33, 50 and 67 (wt. %), respectively.

Characterization

Scanning electron microscopy (SEM) measurements were performed using the Zeiss SIGMA field emission gun (FEG-SEM). The working conditions were accelerating voltage of 1.00 kV and working distance of 2 mm. AFM was performed on thin films coated on silicon wafer with a Bruker Dimension Icon™ in QNM mode and KPFM mode. Silicon probes doped with nitrogen (PFQNE-Al) were used for the investigation, Kn » 0.6 ± 0.1 N/m. Freshly cleaved HOPG was used as reference to measure work function of the tip (4.31 ± 0.04 eV) in ambient air condition at 33% humidity. The V_{CPD} (contact potential

difference) data was recorded at lift height of 10 nm. UV-vis absorption spectra was recorded with Shimadzu UV3600Plus UV-Vis-NIR from 250 nm to 600 nm. Photoluminescence emission spectroscopy was performed on a Shimadzu RF 6000, and time-resolved photoluminescence using a Horiba Deltaflex™ with a 10 mm path-length quartz cuvette with an excitation wavelength of 358 nm. All the PL measurements were carried out with the samples exhibiting the same optical density to be consistent. Raman spectroscopy was carried out with a Renishaw inVia Raman-AFM with an excitation wavelength of 660 nm.

Electrochemical measurements were recorded with a Gamry Reference 600+ potentiostat with glassy carbon as the working electrode (3 mm diameter, BASi), platinum wire as the counter electrode and Ag/AgCl (3M KCl) as the reference electrode in phosphate buffer solution. A volume of 4 mL GO and GO/PIM-1 nanohybrid dispersions was deposited onto the glassy carbon electrode. Cyclic voltammetry experiments were performed (scan rate 10 mV s^{-1}) to investigate the electrochemical reduction of GO in aqueous 0.1 M PBS pH=5. Size distribution measurements were performed with an Anton Paar Litesizer 80 particle analyser.

Results and Discussion

Figure 1**A** schematically illustrates the chemical structures of the component materials. PIM-1 nanoparticles and GO/PIM-1 nanohybrids dispersed in water were synthesised using a re-precipitation method. The polymer is dissolved in a good solvent (THF) which is miscible with an anti-solvent. Mixing of these two dispersions causes the solvated polymer chains to contract and precipitate as solid nanoparticles. Stable dispersions were obtained by this method (see Figure 1**B**, 1**C**) with 1 mg PIM-1 and 0.0, 0.5, 1.0, or 2.0 mg GO in 20 mL water. The morphology of PIM-1 nanoparticles and GO/PIM-1 nanohybrids were studied by scanning electron microscopy (SEM) and atomic force microscopy (AFM). Figure 1**D** shows that uniform PIM-1 nanoparticles are successfully prepared and they are smaller than 100 nm in diameter. For the nanohybrids, Figure 1**E** and 1**F** suggest that PIM-1 nanoparticles formed in GO dispersion tended to graft uniformly to the surface of the GO sheets. The particle size histogram (Figure 1**G**) produced from AFM images of the hybrids is consistent with observations of the pristine PIM-1 nanoparticles.

PIM-1 is a non-conductive molecule with interesting nanoscale structural and optical properties. As such investigation of the optical properties can yield information on the interactions of the PIM-1 chains with one-another and their environment. It has been suggested that inter-molecular interactions, such as hydrogen bonding, could lead to re-arrangement of PIM-1 chains in different molecular environments (as may be produced through the re-precitpitation process), but it is hard to completely confirm[23]. To the best of our knowledge, the effect of chain arrangement of PIM-1 on optical and electronic properties has never been reported. As for other conjugated polymers, there is extensive prior work in the literature[24]. Indeed, our previous work on nanohybrids of poly(3-hexylthiophene) (P3HT) showed evidence for polymer conformational effects in the form of vibronic features in the optical spectroscopy measurements[20]. UV-visible extinction spectra is shown in Figure 2**A** for PIM-1 nanoparticles and for GO/PIM-1 nanohybrids in aqueous dispersion over a wavelength range of 250 to 600 nm. In agreement with previously reported data[11], two intense peaks are observed for PIM-1. The peak centred around 291 nm corresponds to the σ–π^* transition and the peak centred at 429 nm arises from a π-π^* transition, which is commonly observed for conjugated aromatic compounds. In the hybrid materials, both absorption peaks for PIM-1 are observed to be diminished, and slightly red-shifted with increasing GO content (see also Figure **S1** for a second derivative plot of the data in Figure 2**A**). The inset in Figure 2**A** shows the optical bandgaps of the component materials derived from Tauc plots (see figure **S2**) of the UV-Vis spectra. We observe a negligible trend in the optical gap with increasing GO content in the hybrids, suggesting that there is no strong structural or chemical interactions of the component materials. This suggests the observed peak shift of the PIM-1 UV-Vis features is likely due to increased scattering due to the GO addition[24].

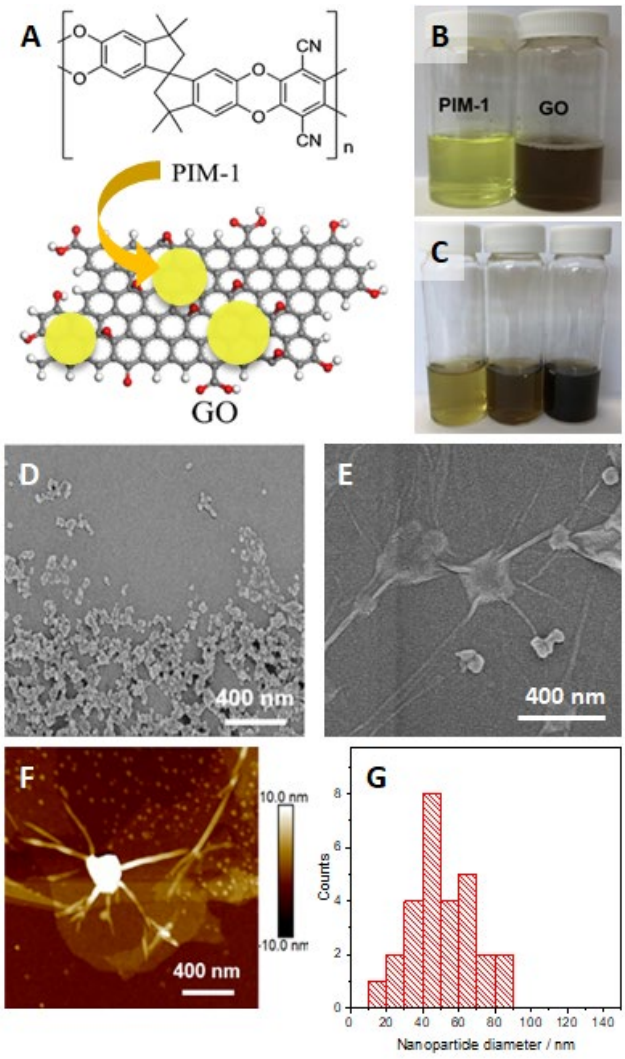

Figure 1. **A**: Molecular structure of PIM-1 and schematic illustrating the formation of GO/PIM-1 charge transfer nanohybrid materials. **B**: Photographs of aqueous dispersions of PIM-1 nanoparticles and GO. **C**: Photographs of the GO/PIM-1 nanohybrids with 33, 50 and 67 wt. % GO from left to right. **D**: Scanning electron micrograph of PIM-1 nanoparticles on a silicon wafer, and **E**: GO/PIM-1 (50 wt.%) nanohybrid. **F**: Atomic force micrograph of the nanohybrid in **E**. **G**: Particle size histogram from AFM for the GO/PIM-1 nanohybrid.

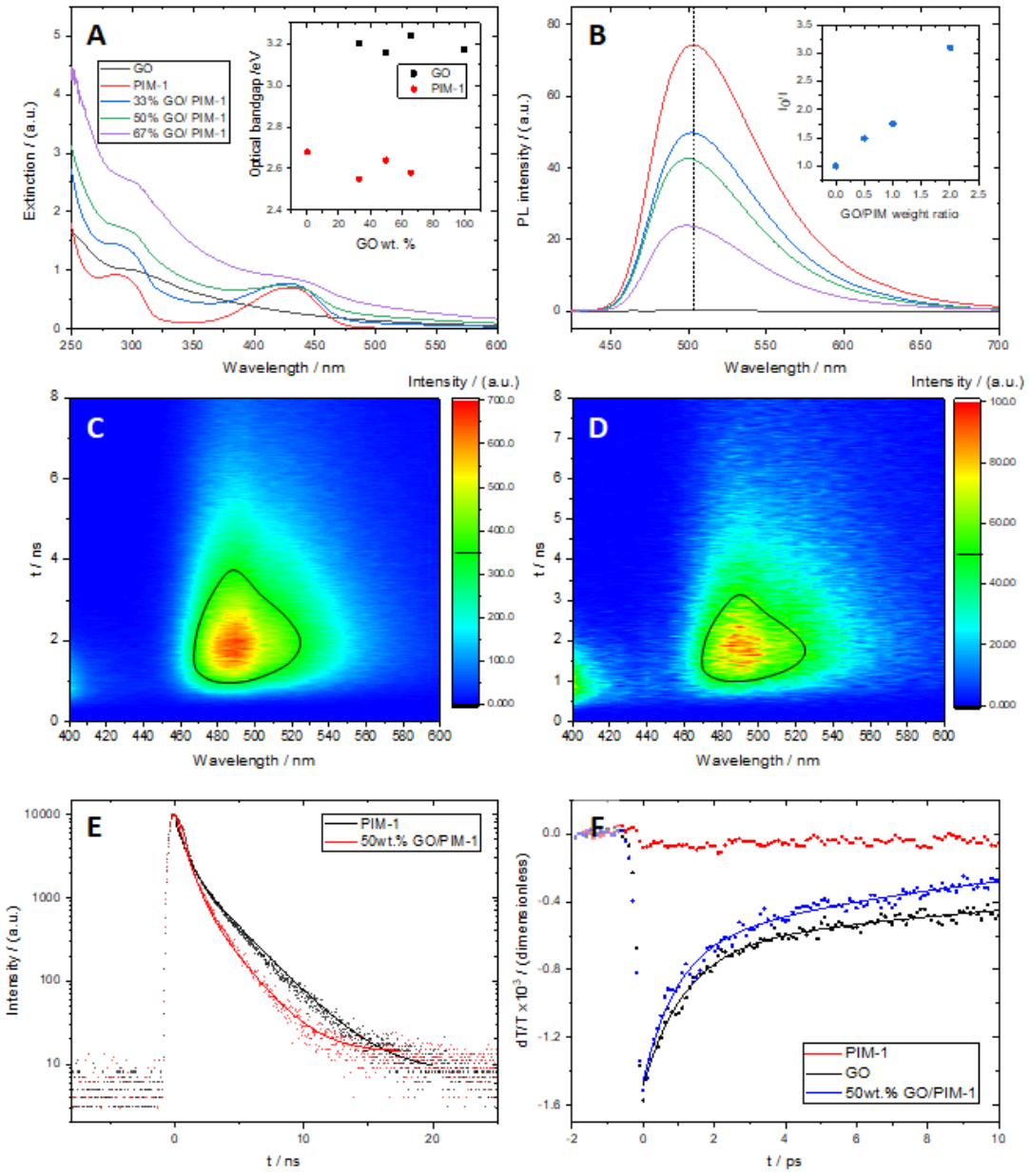

Figure 2. **A**: UV-vis extinction spectra for GO, PIM-1 nanoparticles and GO/PIM-1 nanohybrids in aqueous dispersion. (Inset) Optical bandgap energies for the component materials in all dispersions, measured from Tauc plots. **B**: Steady-state fluorescence data (λ_{ex} = 358 nm) for PIM-1 nanoparticles and GO/PIM-1 nanohybrids. (Inset) Relative fluorescence intensity versus the GO/PIM-1 weight ratio. Time-resolved emission spectral data for PIM-1 nanoparticles (**C**) and GO-PIM-1 nanohybrids (**D**). The black contour denotes 50% of the peak intensity in both cases. **E**: Single-wavelength time-resolved fluorescence decay curve (λ_{ex} = 358 nm, λ_{em} = 510 nm) for PIM-1 nanoparticles and GO/PIM-1 nanohybrids. **F**: Transient differential transmission curves for GO, PIM-1 nanoparticles and for GO/PIM-1 hybrids as a function of pump-probe delay with 400 nm pump (5.4 GW/cm²) and 800 nm probe (0.6 GW/cm²).

PIM-1 exhibits strong fluorescence due to the presence of conjugated ring groups within the polymer backbone[25] (see Figure 1**A**). The spectra in Figure 2**B** show that the fluorescence intensity is quenched by the presence of GO (see also Figure **S3**). The inset in Figure 2**B** shows that the peak intensity scales approximately linearly with GO/PIM-1 ratio. Additionally, the emission peak is significantly blue-shifted (see also a Gaussian deconvolution in Figure **S4**), which indicates a strong interaction between these two materials[26]. Since there is no significant change to the PIM-1 optical gap we can reason that the decrease in the Stokes shift (see also emission and excitation spectra in Figure **S5**) in the hybrid indicates a decrease in the exciton binding energy[25]. The Stokes shift is approximately 200 meV in the pristine PIM and is reduced by ~75 meV in the hybrid. In many conjugated systems the Stokes shift, determined from the difference in energy of the absorption edge and emission energy, is found to decrease as the rigidity of the polymer backbone is increased. Similar effects may be responsible for the observed decrease in Stokes shift in the nanohybrids. Moreover, the energy gap for an electronic transition of a chromophore is influenced by the fluctuations in the environment. In our hybrid systems, as the GO content increases, it may be that the associated reduction in Stokes shift can be explained by a steric interaction of the PIM-1 adsorbed onto the GO.

Figure 2**C** and 2**D** show the time-resolved emission spectra under 358 nm excitation. Although it is not the optimum excitation for this measurement, the energy is above the optical gap and as such can still produce excited carriers, which relax non-radiatively before PL emission. In addition, the lower emission intensity doesn't influence the PL lifetime measurement for the same emission energy between the excited state and the ground state. Both plots have a contour shown at 50% intensity (relative to peak emission) which show that the hybrid lifetime is reduced over the whole emission range. Since the maximum position of the fluorescence peak is at 510 nm for excitation at 358 nm, Figure 2**E** shows the temporal decay curves at this wavelength (λ_{em} = 510 nm) for both the PIM-1 nanoparticles and the GO/PIM-1 nanohybrid. The decay data for the pristine nanoparticles is best fitted to a double-exponential function with component lifetimes of τ_1=0.66 ns and τ_2=2.66 ns. Delocalisation of the electron-hole pair across two chains gives longer-lived PL while the exciton confined to single chain gives short-lived PL. This is due to an increase in electron-hole wavefunction overlap (and hence recombination probability) for decreasing binding radius. Therefore, we attribute the two component lifetimes to intra- and inter-chain emission, respectively. In the hybrids, the short-lived intra-chain component is unmodified while the long-lived inter-chain component reduces in intensity and lifetime[20,27, 28]. As such we observe a consistent reduction of the total PL lifetime of GO/PIM-1 nanohybrids with increasing mass ratios (33, 50, 67 wt.% GO) (see Figure **S6**).

The photophysical properties of the nanohybrids were further investigated by pump-probe transient absorption measurements (Figure 2**F**). In this technique a pump pulse (at 400 nm) is employed to generate a population of electrons in an excited state which are then probed with delayed pulses (at 800 nm) to investigate the effect of the modified electron population on the transient absorption. This method facilitates investigation of the short-time carrier dynamics in the GO and how the addition of the PIM-1 modifies this behaviour. Since PIM-1 does not contain extended conjugated segments, charges elevated to excited states by the pump pulse do not contribute to the optical behaviour below the HOMO-LUMO transition energy; this results in the negligible change in sample transmittance observed in Figure 2**F**. In GO charges elevated by the pump pulse are free to move due to extended (though not globally connected) conjugated regions. This carrier mobility means that the generated population of carriers acts as a free electron gas, increasing the sample reflectance (and lowering the transmittance) at the probe photon energy, which is below the bandgap of the material. Depopulation of this excited state, and therefore recovery of the sample transmittance, can occur by recombination of the electron-hole pairs or by charge trapping. The data for both pristine GO and the nanohybrid were fitted with double exponential functions (shown in Figure 2**F**). For the pristine GO the time constants τ_1 and τ_2 were 1.15 ps and 23.6 ps, respectively. For the GO/PIM-1 nanohybrid the corresponding values were τ_1=0.94 ps and τ_2=11.4 ps. A significant decrease in the transient state lifetime of GO with the presence of adsorbed PIM-1 nanoparticles is noted, suggesting an increase in recombination rate as carriers become trapped by PIM states through non-radiative energy loss (and are subsequently able to undergo radiative relaxation)[26].

Given the spectroscopic evidence of excited state charge transfer between the two materials in the nanohybrid, we applied other characterisation techniques to elucidate the presence of any ground state interactions. Raman spectroscopy is convenient for this purpose, as it has been demonstrated that electronic doping of the extended conjugated regions of graphene materials causes reproducible shifts to their characteristic Raman features[29, 30]. The Raman spectrum (660 nm excitation) for PIM-1 nanoparticles is shown in Figure 3**A**. There are several modes in the range between 1300 and 1700 cm^{-1}, which are consistent with the reported Raman spectrum for PIM-1[31] and arise from the conjugated ring species present in the polymer backbone (see Figure 1**A**). An intense mode at 2236 cm^{-1} is attributed to C≡N bond stretching, and the broad feature centred at 2900 cm^{-1} can be attributed to the various C-H stretches[32].

Figure 3**B** compares normalised Raman spectra of GO and the GO/PIM-1 nanohybrids. For GO the typical D-peak at 1335 cm^{-1} and G-peak at 1590 cm^{-1} are observed in addition to the 2D peak at 2680 cm^{-1} and the D+G peak at 2880 cm^{-1} [33]. An increase in intensity is observed of the D+G peak in the nanohybrids is due to overlap with the C-H band in the polymer[30]. The stiffening of the G peak (by nearly 6 cm^{-1}) indicates a charge transfer process[34]. The significant softening of both D- (15 cm^{-1}) and 2D-peaks (30 cm^{-1}) indicates effective p-doping of the GO, as observed in other work on defective graphene[35]. In the literature softening of 2D peak with decrease in carrier concentration (lowering of the Fermi energy, corresponding to p-doping of the GO), which is observed in our data, is noted. However for pristine, defect-free graphene systems, the opposite effect is indicated (softening of the D and 2D modes indicates n-doping)[33]. The difference in behavior of the D and 2D modes appears to be related to the nature of the defects within the carbon lattice that are prevalent in graphene oxide but not observed in pristine graphene.

Figure 3**C** and 3**D** show Raman mapping of the hybrids (over a 25x25 µm area) for the peak intensity at 2236 cm^{-1} and G-peak position, respectively. Clearly visible is a correlation between the intensity of the PIM feature and the G-peak shift in the GO. Figure 3**E** plots the G-peak position against the peak intensity at 2236 cm^{-1} using pixel-wise data from Figure 3**C** and **D**. This data is binned and averaged to clarify the overall trend. Additionally, a line is shown as a 'guide to the eye', based on G-peak positions in point spectra of the pristine GO and hybrid. According to the equation[36], $\hbar w_G = \alpha' |\varepsilon_F| = \alpha' \sqrt{n_d \pi} \hbar v_F$(where ε_F is the Fermi energy, n_d is the doping density, $\hbar v_F$=5.52 eV, and $\alpha' = 4.39 \times 10^{-3}$ at 0 K), the shift in the G-peak can be used to estimate the doping density, resulting in a value of 2.25×10[12] cm^{-2}. From this value it is possible to estimate the resultant shift of the work function of the nanohybrid[37] as 75 meV. This prediction of the modification to the work function can be experimentally investigated through the use of Kelvin Probe Force Microscopy (KPFM).

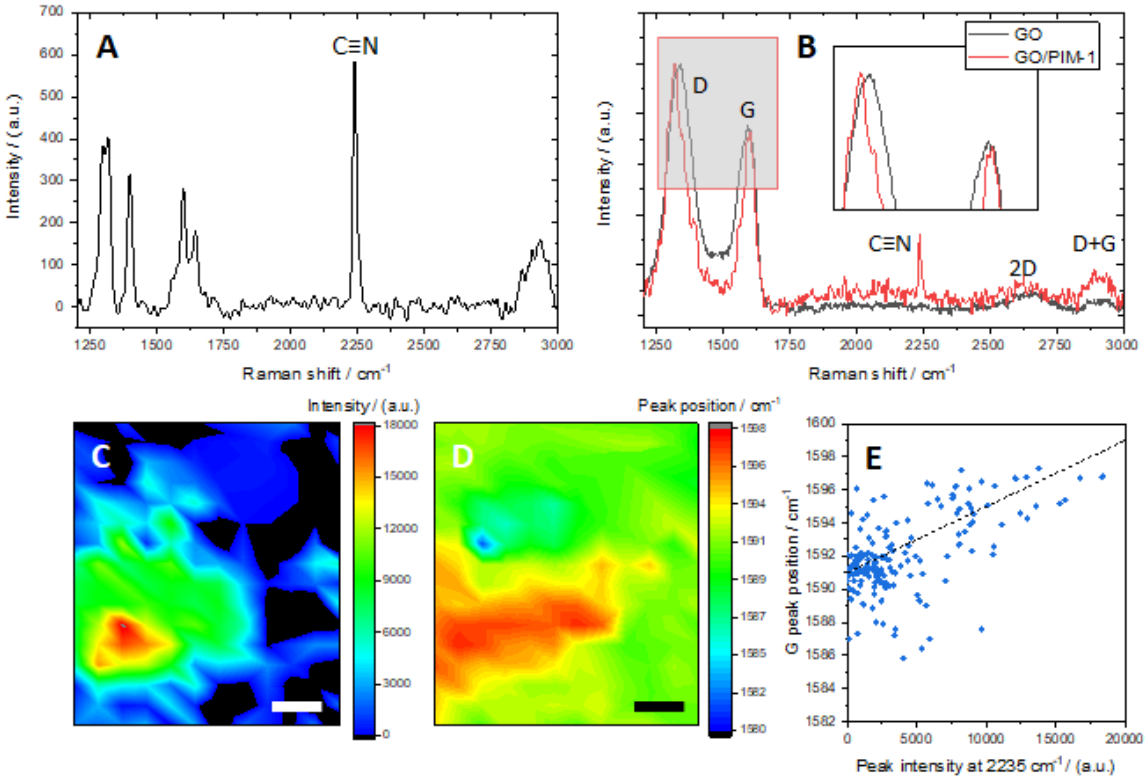

Figure 3. **A**: Raman spectrum for PIM-1 nanoparticles (λ_{ex} = 660 nm). **B**: Comparison of normalised Raman data for GO and GO/PIM-1. The highlighted area is enlarged in the inset, for clarity. **C**, **D**: Raman mapping for GO/PIM-1 nanohybrids, showing the peak intensity at 2236 cm^{-1} and G peak position, respectively. Scale bars are 5 µm. **E**: Pixelwise correlation analysis of the G peak position and the peak intensity at 2236 cm^{-1} for GO/PIM-1 nanohybrids. The line shown is a guide to the eye based on observed G peak shifts in low-magnification point spectra.

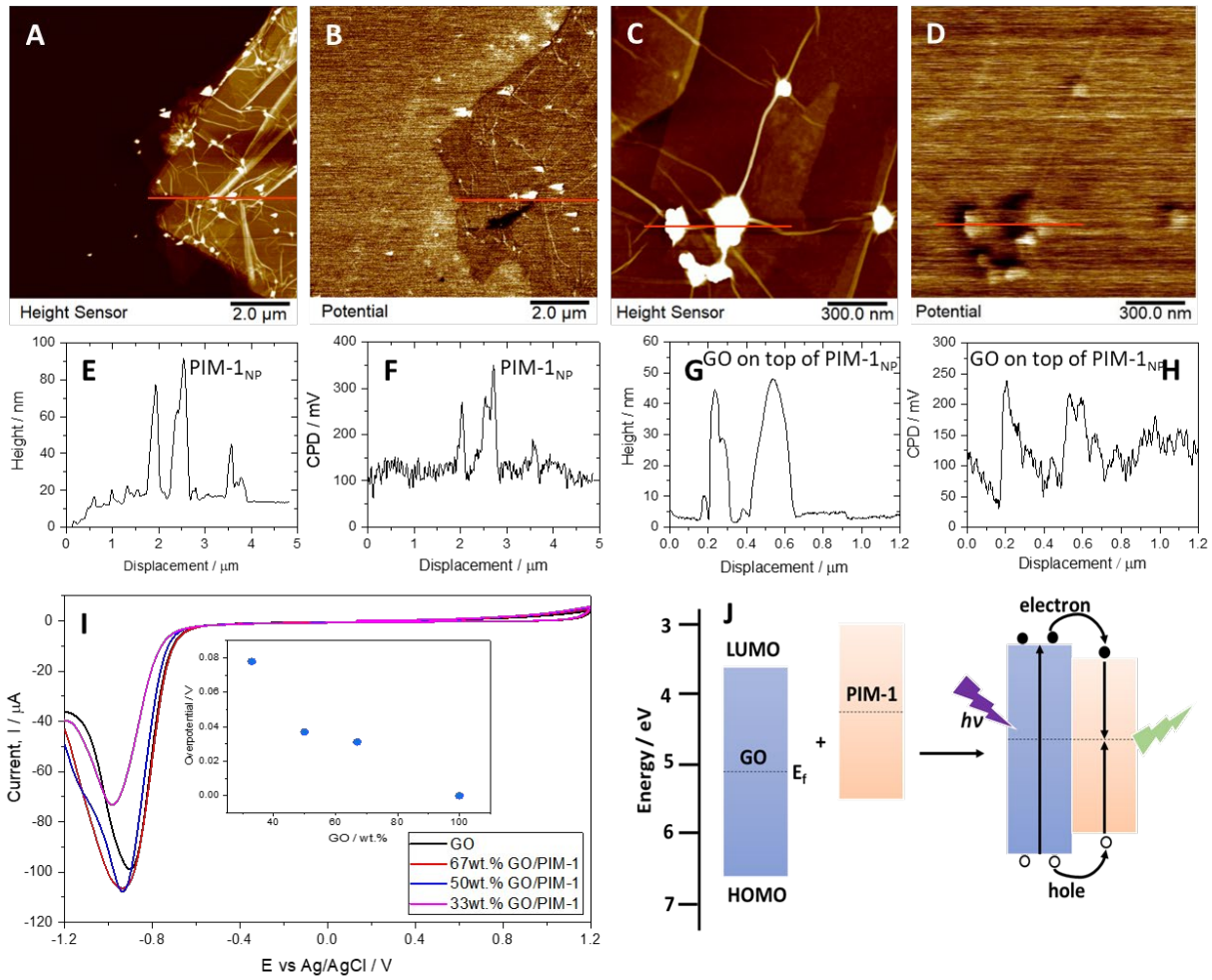

Figure 4. **A**, **B**: AFM topography and KPFM (respectively) of the GO/PIM-1 nanohybrid. **C** and **D**: AFM topography and KPFM of GO sheets on top of "wrapped" PIM-1 nanoparticles. **E**, **G**: Height and CPD line profiles of PIM-1 nanoparticles on top of the GO sheet, from the data in **A** and **B** respectively. **G**, **H**: Height and CPD line profiles of GO sheets on top of the "wrapped" PIM-1 nanoparticles, from the data in **C** and **D** respectively. **I**: Electrochemical reduction for GO and GO/PIM-1 nanohybrids deposited onto a glassy carbon electrode in phosphate buffer solution (pH 5, 1st cycle, scan rate 10 mV s^{-1}). (Inset) Overpotential of GO reduction against GO/PIM-1 weight ratio. **J**: Schematic energy level diagram of the isolated materials and nanohybrid.

KPFM is a scanning probe technique that measures the local contact potential difference (V_{CPD}, in mV) between the probe and sample. The CPD relates to the surface charges formed as a result of Fermi level alignment between the tip and sample materials (through external circuit connections). The value of V_{CPD} can be directly related to the work functions ϕ of the two materials in question by $V_{CPD} = (\phi_{sample} - \phi_{tip})/e$, where e is the electronic charge[38]. Either by use of a tip with calibrated work function, or by examining measurements relative to a common material in multiple samples (such as the silicon substrate), it is possible to infer relative changes to the work functions in the nanohybrids by comparison to the pristine materials.

Figure 4**A** and **B** show AFM topography and KPFM contact potential difference (CPD) maps of the nanohybrids where the PIM-1 nanoparticles appear on top of the GO sheet. Figure 4**C** and **D** show equivalent data for a region of the sample where the GO sheet lays on top of the nanoparticles. The line sections marked in Figure 4**A** to **D** are plotted in Figure 4**E** to **H**. We observe from the height profiles in both cases (Figure 4**E** and **G**) that the nanoparticles have diameters consistent with the histogram presented in Figure 1**G**. For the PIM-on-GO samples in Figure 4**A** and 4**B**, the GO is measured as having V_{CPD} around 100 mV, while the PIM-1 nanoparticles are measured to have V_{CPD} between 200 and 350 mV. This is taken to be representative of the pristine materials due to their separation when probing the surface of the PIM-1. By contrast, GO is atomically thin and has non-negligible conductivity[39], meaning that the influence of the PIM-1 on the V_{CPD} can be

determined by measuring GO-on-PIM samples. The isolated area of GO in Figure 4**C** and **D** have broadly similar V_{CPD} as in the PIM-on-GO samples, while V_{CPD} of GO in the presence of wrapped PIM-1 nanoparticles is found to increase to around 200 mV (Figure 4H). This can be interpreted as a modification to the work function of the GO sheet due to doping by the underlying PIM-1 nanoparticle. This work function modification is in agreement with the shift calculated from the doping density determined Raman spectroscopy, suggesting the GO is indeed p-doped by a charge transfer interaction with the PIM-1.

For electrochemical measurements (see Figure 4**I**), a volume of 4 mL GO and GO/PIM-1 nanohybrid was deposited onto a glassy carbon electrode. Cyclic voltammetry was performed to study the electrochemical reduction of GO in aqueous 0.1 M phosphate buffer solution (PBS) at pH 5. The reduction of GO is observed as a chemically irreversible process, which is in agreement with references[40]. Therefore, the 1st linear potential sweeps were recorded for comparison. Clear and sharp peaks are observed in all cases. For the GO/PIM-1 nanohybrids, the shape of the peak shows some broadening consistent with a kinetic barrier to the GO-to-graphene transition due to surface coverage of the GO by PIM-1. The underlying mechanism for the electron transfer is due to the relative energies of states in the electrode and the species. If the Fermi level in the electrode is higher than the lowest unoccupied molecular orbital (LUMO) of the species, electrons will be transferred from the electrode to the species, resulting reduction of the species. Therefore, since the overpotential for the GO/PIM-1 nanohybrids (plotted in the inset to Figure 4**I**) increases with increasing PIM-1 content, we can infer a lowering of the Fermi energy and corroborates the observation of p-doping of the GO[20] through the other measurement techniques above. Finally, The LUMO energy can be calculated from the onset reduction potential as E (LUMO) =-e $[E_{red}^{onset} + 4.4]$[41], so the LUMO energy of the GO is estimated as 3.6 eV.

Based on the measurements presented, a simple model of the charge transfer interaction in the hybrid system can be illustrated as in Figure 4**J**. From the literature[11,37], the HOMO (5.5 eV) and LUMO (3.0 eV) levels in PIM-1 are higher than GO (6.6 eV, 3.6 eV) in good agreement with the values presented here, where measured. In addition, the alignment of their Fermi levels in the hybrid presents the possibility of intermolecular exciton diffusion due to the narrower bandgap in the polymer. The photo-excited electrons and holes generated in the GO (~350 nm) can be injected into PIM-1 in an exciton transfer process. Subsequently, the exciton can recombine in the PIM-1 to emit in the green (~500 nm). While this doesn't account for the extrinsic nature of these semiconductors (n-type PIM-1 and p-type GO)[42], it is even possible that bound excitons are delocalised across the interface of the materials with electrons preferentially transferred to the PIM-1 and holes remaining in (and resulting in doping of) the GO until recombination. The ability to design such charge transfer complexes on the nanoscale is important and application of effects at this length scale are most likely in sensing and catalysis where charging can translate into chemical effects, for example in promotion effects in catalysis.

Conclusion

In this report, we prepare GO/PIM-1 nanohybrid charge transfer materials through a facile re-precipitation approach. By this method, PIM-1 nanoparticles form and associate with GO sheets in dispersion, resulting in the nanohybrid materials. Microscopy analysis by both SEM and AFM reveal uniformly dispersed nanoparticles attached to the GO surface. The optical properties of the GO/PIM-1 nanohybrids are investigated using UV-Visible extinction, steady-state and time-resolved photoluminescence spectroscopies, Raman spectroscopy, and pump-probe transient absorption spectroscopy. We conclude from these techniques that there are both excited state and ground state charge transfer effects present. Kelvin probe force microscopy and electrochemical measurements provide direct evidence for ground state charge transfer causing a shift in Fermi level of the GO component in the nanohybrids. In summary, graphene oxide is p-doped while PIM-1 is n-doped in the GO/PIM-1 nanohybrids. The resulting charging effects are chemically significant and could be important in other fields such as in gas adsorption and separation, in membrane development, and in sensing and catalysis.

Associated Content

Supporting Information

Second derivative of UV-Vis spectra, steady-state photoluminescence excitation (PLE) maps, Emission/Excitation spectra, UV-Vis and steady-state fluorescence, Tauc plots, Time-resolved fluorescence delay curves, Gaussian fitting for the fluorescence emission peak, FTIR spectra.

Author Information

Corresponding Author

Matthew Large: M.Large@sussex.ac.uk

Alan Dalton: A.B.Dalton@sussex.ac.uk

Acknowledgements

This work is supported by strategic development funding from the University of Sussex.

References

(1) Vandewal, K.; Albrecht, S.; Hoke, E. T.; Graham, K. R.; Widmer, J.; Douglas, J. D.; Schubert, M.; Mateker, W. R.; Bloking, J. T.; Burkhard, G. F.; et al. Efficient Charge Generation by Relaxed Charge-Transfer States at Organic Interfaces. *Nat. Mater.* **2014**, *13* (1), 63–68.

(2) Coropceanu, V.; Cornil, J.; da Silva Filho, D. A.; Olivier, Y.; Silbey, R.; Brédas, J. L. Charge Transport in Organic Semiconductors. *Chem. Rev.* **2007**, *107* (4), 926–952.

(3) Sirringhaus, B. H. Device Physics of Solution-Processed Organic Field-Effect Transistors . *Adv. Mater.* **2005**, No. 17, 2411–2425.

(4) Gélinas, S.; Rao, A.; Kumar, A.; Smith, S. L.; Chin, A. W.; Clark, J.; Poll, T. S. Van Der; Bazan, G. C.; Friend, R. H. Ultrafast Long-Range Charge Photovoltaic Diodes. **2014**, *343* (January), 512–517.

(5) Bates, M. K.; Jia, Q.; Doan, H.; Liang, W.; Mukerjee, S. Charge-Transfer Effects in Ni-Fe and Ni-Fe-Co Mixed-Metal Oxides for the Alkaline Oxygen Evolution Reaction. *ACS Catal.* **2016**, *6* (1), 155–161.

(6) Liao, F.; Lo, T. W. B.; Qu, J.; Kroner, A.; Dent, A.; Tsang, S. C. E. Tunability of Catalytic Properties of Pd-Based Catalysts by Rational Control of Strong Metal and Support Interaction (SMSI) for Selective Hydrogenolyic C-C and C-O Bond Cleavage of Ethylene Glycol Units in Biomass Molecules. *Catal. Sci. Technol.* **2015**, *5* (7), 3491–3495.

(7) Zheng, W.; Jones, S.; Hong, X.; Tsang, S. C. E. Photo and Electronic Excitation for Low Temperature Catalysis over Metal Nanoparticles Using an Organic Semiconductor. *RSC Adv.* **2014**, *4* (88), 47488–47496.

(8) Budd, P. M.; Ghanem, B. S.; Makhseed, S.; McKeown, N. B.; Msayib, K. J.; Tattershall, C. E. Polymers of Intrinsic Microporosity (PIMs): Robust, Solution-Processable, Organic Nanoporous Materials. *Chem. Commun.* **2004**, No. 2, 230–231.

(9) Ghanem, B. S.; McKeown, N. B.; Budd, peter M.; Fritsch, D. Polymers of Intrinsic Microporosity Derived from Bis(Phenazyl) Monomers. *Macromolecules* **2008**, *41* (5), 1640–1646.

(10) Chaukura, N. Interaction of a Polymer of Intrinsic Microporosity (PIM-1) with Penetrants. *Am. J. Appl. Chem.* **2015**, *3* (3), 139.

(11) Gupta, B. K.; Kedawat, G.; Kumar, P.; Rafiee, M. A.; Tyagi, P.; Srivastava, R.; Ajayan, P. M. An N-Type, New Emerging Luminescent Polybenzodioxane Polymer for Application in Solution-Processed Green Emitting OLEDs. *J. Mater. Chem. C* **2015**, *3* (11), 2568–2574.

(12) Song, J.; Du, N.; Dai, Y.; Robertson, G. P.; Guiver, M. D.; Thomas, S.; Pinnau, I. Linear High Molecular Weight Ladder Polymers by Optimized Polycondensation of Tetrahydroxytetramethylspirobisindane and 1,4-Dicyanotetrafluorobenzene. *Macromolecules* **2008**, *41* (20), 7411–7417.

(13) Pei, S.; Cheng, H. M. The Reduction of Graphene Oxide. *Carbon N. Y.* **2012**, *50* (9), 3210–3228.

(14) Eda, G.; Chhowalla, M. Chemically Derived Graphene Oxide: Towards Large-Area Thin-Film Electronics and Optoelectronics. *Adv. Mater.* **2010**, *22* (22), 2392–2415.

(15) Loh, K. P.; Bao, Q.; Eda, G.; Chhowalla, M. Graphene Oxide as a Chemically Tunable Platform for Optical Applications. *Nat. Chem.* **2010**, *2* (12), 1015–1024.

(16) Loh, K. P.; Bao, Q.; Ang, P. K.; Yang, J. The Chemistry of Graphene. *J. Mater. Chem.* **2010**, *20* (12), 2277–2289.

(17) Vallés, C.; Jiménez, P.; Muñoz, E.; Benito, A. M.; Maser, W. K. Simultaneous Reduction of Graphene Oxide and Polyaniline: Doping-Assisted Formation of a Solid-State Charge-Transfer Complex. *J. Phys. Chem. C* **2011**, *115* (21), 10468–10474.

(18) Stylianakis, M. M.; Stratakis, E.; Koudoumas, E.; Kymakis, E.; Anastasiadis, S. H. Organic Bulk Heterojunction Photovoltaic Devices Based on Polythiophene-Graphene Composites. *ACS Appl. Mater. Interfaces* **2012**, *4* (9), 4864–4870.

(19) Liu, Q.; Liu, Z.; Zhang, X.; Yang, L.; Zhang, N.; Pan, G.; Yin, S.; Chen, Y.; Wei, J. Polymer Photovoltaic Cells Based on Solution-Processable Graphene and P3HT. *Adv. Funct. Mater.* **2009**, *19* (6), 894–904.

(20) Istif, E.; Hernández-ferrer, J.; Urriolabeitia, E. P.; Stergiou, A.; Tagmatarchis, N.; Fratta, G.; Large, M. J.; Dalton, A. B.; Benito, A. M.; Maser, W. K. Conjugated Polymer Nanoparticle – Graphene Oxide Charge-Transfer Complexes. *Adv. Funct. Mater*. **2018**, *1707548*, 1–10.

(21) Chen, M.; Soyekwo, F.; Zhang, Q.; Hu, C.; Zhu, A.; Liu, Q. Graphene oxide nanosheets to improve permeability and selectivity of PIM-1 membrane for carbon dioxide separation. *J. Ind. Eng. Chem.* **2018**, 63, 296-302.

(22) Aliyev, E. M.; Khan, M. M.; Nabiyev, A. M.; Alosmanov, R. M.; Bunyad-zadeh, I. A.; Shishatskiy, S.; Filiz, V. Covalently Modified Graphene Oxide and Polymer of Intrinsic Microporosity (PIM-1) in Mixed Matrix Thin-Film Composite Membranes. *Nanoscale. Res. Lett*. **2018**, *13*, 359–372.

(23) Weber, J.; Du, N.; Guiver, M. D. Influence of Intermolecular Interactions on the Observable Porosity in Intrinsically Microporous Polymers. *Marcromolecules*. 2011, 44, 1763–1767.

(24) Kim, J.; Swager, T. M. Control of Conformational and Interpolymer Effects in Conjugated Polymers. *Nature* **2001**, *413* (6855), 548.

(25) Seo, J.; Kim, S.; Park, S. Y. Strong Solvatochromic Fluorescence from the Intramolecular Charge-Transfer State Created by Excited-State Intramolecular Proton Transfer. *J. Am. Chem. Soc.* **2004**, *126* (36), 11154–11155.

(26) Noone, K. M.; Subramaniyan, S.; Zhang, Q.; Cao, G.; Jenekhe, S. A.; Ginger, D. S. Photoinduced Charge Transfer and Polaron Dynamics in Polymer and Hybrid Photovoltaic Thin Films: Organic vs Inorganic Acceptors. *J. Phys. Chem. C* **2011**, *115* (49), 24403–24410.

(27) Jennings, T. L.; Singh, M. P.; Strouse, G. F. Fluorescent Lifetime Quenching near d = 1.5 Nm Gold Nanoparticles: Probing NSET Validity. *J. Am. Chem. Soc.* **2006**, *128* (16), 5462–5467.

(28) Khan, S.; Gupta, A.; Verma, N. C.; Nandi, C. K. Time-Resolved Emission Reveals Ensemble of Emissive States as the Origin of Multicolor Fluorescence in Carbon Dots. *Nano Lett.* **2015**, *15*, 8300–8305.

(29) Panchakarla, B. L. S.; Subrahmanyam, K. S.; Saha, S. K.; Govindaraj, A.; Krishnamurthy, H. R.; Waghmare, U. V; Rao, C. N. R. Synthesis , Structure , and Properties of Boron- and Nitrogen-Doped Graphene. Adv. Mater. 2009, 560012 (21), 4726–4730.

(30) Rao, A. M.; Eklund, P. C.; Bandow, S.; Thess, A. Evidence for Charge Transfer in Doped Carbon Nanotube Bundles from Raman Scattering. Nature 1997, 388, 257–259.

(31) Shin, Y.; Prestat, E.; Zhou, K. G.; Gorgojo, P.; Althumayri, K.; Harrison, W.; Budd, P. M.; Haigh, S. J.; Casiraghi, C. Synthesis and Characterization of Composite Membranes Made of Graphene and Polymers of Intrinsic Microporosity. *Carbon N. Y.* **2016**, *102*, 357–366.

(32) L.; Yu, Y.; Lin, K.; Zhou, X.; Wang, H.; Liu, S.; Ma, X. New C- H Stretching Vibrational Spectral Features in the Raman Spectra of Gaseous and Liquid Ethanol. J. Phys. Chem. C 2007, 111, 8971–8978.

(33) Saravanan, K.; Jayalakshmi, G.; Suresh, K.; Sundaravel, B.; Panigrahi, B. K.; Phase, D. M. Structural Evaluation of Reduced Graphene Oxide in Graphene Oxide during Ion Irradiation: X-Ray Absorption Spectroscopy and in-Situ Sheet Resistance Studies. *Appl. Phys. Lett.* **2018**, *112* (11).

(34) Avinash, M. B.; Subrahmanyam, K. S.; Sundarayya, Y.; Govindaraju, T. Covalent Modification and Exfoliation of Graphene Oxide Using Ferrocene. *Nanoscale* **2010**, *2* (9), 1762–1766.

(35) Bruna, M.; Ott, A. K.; Ijas, M.; Yoon, D.; Sassi, U.; Ferrari, A. C. H. Doping Dependence of the Raman Spectrum of Defected Graphene. *ACS. Nano.* 2014, 8, 7432-7441.

(36) Kim, S. J.; Park, S. J.; Kim, H. Y.; Jang, G. S.; Park, D. J.; Park, J.; Lee, S.; Ahn, Y. H. Characterization of chemical doping of graphene by in-situ Raman spectroscopy. *Appl. Phys. Lett*. 2016, 108, 203111.

(37) Das, A.; Pisana, S.; Chakraborty, B.; Piscanec, S.; Saha, S. K.; Waghmare, U. V; Novoselov, K. S.; Krishnamurthy, H. R.; Geim, A. K.; Ferrari, A. C.; et al. Monitoring Dopants by Raman Scattering in an Electrochemically Top-Gated Graphene Transistor. **2008**, *3* (April), 1–6.

(38) Samaddar, S.; Coraux, J.; Martin, S. C.; Grévin, B.; Courtois, H.; Winkelmann, C. B. Equal Variations of the Fermi Level and Work Function in Graphene at the Nanoscale. *Nanoscale* **2016**, *8* (33), 15162–15166.

(39) Marsden, A. J.; Papageorgiou, D. G.; Valles, C.; Liscio, A.; PaLERMO, V.; Bissett, M. A.; Young, R. J.; Kinloch, I. A.; Electrical Percolation in Graphene–Polymer Composites. *2D Materials*. 2018, 5,032003.

(40) Mani, V.; Devades, B.; Chen, S. Direct Electrochemistry of Glucose Oxidase at Electrochemically Reduced Graphene Oxide-Multiwalled Carbon Nanotubes Hybrid Material Modified Electrode for Glucose Biosensor. *Biosens Bioelectron*. 2012, 41, 309–315.

(41) Leonat, L.; Sbarcea, G.; Branzoi, I. V. Cyclic Voltammetry for Energy Levels Estimation of Organic Materials. *U.P.B. Sci. Bull* 2013, 3, 111–118.

(42) Zheng, F.; Xu, W.; Jin, H.; Hao, X.; Ghiggino, K. P. Charge Transfer from Poly(3-Hexylthiophene) to Graphene Oxide and Reduced Graphene Oxide. *RSC Adv*. 2015, 89515–89520.

Table of Contents Graphic